China Ocean Eng., 2021, Vol. 35, No. 2, P. 215–227
DOI: https://doi.org/10.1007/s13344-021-0019-y, ISSN 0890-5487
http://www.chinaoceanengin.cn/ E-mail: coe@nhri.cn

Experimental Investigation on Vortex-Induced Vibration of Deep-Sea Risers of Different Excitation Water Depths

LI Peng[a, b, *], DONG Zheng-kai[a, b], LIU Yu[a, b], WANG Yu[a, b], CONG Ai-jun[a, b], GUO Hai-yan[c], FU Qiang[d]

[a] College of Civil Engineering and Architecture, Shandong University of Science and Technology, Qingdao 266590, China

[b] Shandong Provincial Key Laboratory of Civil Engineering Disaster Prevention and Mitigation, Qingdao 266590, China

[c] College of Engineering, Ocean University of China, Qingdao 266100, China

[d] Yantai CIMC Raffles Ocean Engineering Co., Ltd., Yantai 264000, China

Received May 30, 2020; revised January 17, 2021; accepted February 23, 2021

Abstract

The vortex-induced vibration test of the deep-sea riser was carried out with different excitation water depths in the wave-current combined water flume. By dimensionally changing the multi-stage water depth and hydrodynamic parameters such as outflow velocity at various water depths, the dynamic response parameters such as dominant frequency, dimensionless displacement and vibration trajectory evolution process of the riser under different excitation water depths were explored to reveal the sensitive characteristics of the dynamic response of vortex-induced vibration of the risers under different excitation water depths. The results show that different excitation water depths will change the additional mass of the riser and the fluid damping and other parameters, which will affect the spatial correlation and stability of the vortex shedding behind the riser. In the lock-in region, the distribution range of the characteristic frequency becomes narrow and centered on the lock-in frequency. The increase of the excitation water depth gradually advances the starting point of the lock-in region of the riser, and at the same time promotes the excitation of the higher-order vibration frequency of the riser structure. Within the dimensionless excitation water depth, the dominant frequency and dimensionless displacement are highly insensitive to the excitation water depth at high flow velocity. The change of the excitation water depth will interfere with the correlation of the non-linear coupling of the riser. The "8-shaped" gradually becomes irregular, and the vibration trajectories of the riser show "O-shape", "X-shape" and "Crescent-shape".

Key words: deep-sea riser, excitation water depth, vortex-induced vibration (VIV), dynamic response, coupling effect

Citation: Li, P., Dong, Z. K., Liu, Y., Wang, Y., Cong, A. J., Guo, H. Y., Fu, Q., 2021. Experimental investigation on vortex-induced vibration of deep-sea risers of different excitation water depths. China Ocean Eng., 35(2): 215–227, doi: https://doi.org/10.1007/s13344-021-0019-y

1 Introduction

The deep-sea pipeline structure (referred to as "riser") is used to connect offshore platform and seabed wellhead. It is the basic device for transporting oil and gas from seabed wellhead to platform and is also a relatively complicated structure in the deep-sea oil and gas development system (Gao et al., 2015; Song et al., 2018; Liu et al., 2018). During the operation of the deep-sea oil and gas development system, high-pressure oil or airflow usually passes through the inside of the riser, and the outside needs to bear the action of complex marine environment load such as wave, current, ice and earthquake. At the same time, a platform is connected to the top, and the bottom interacts with the seabed, which will expose the riser to harsh service environment and extremely complex forces and will also increase the construction cost. Forced excitation vibration occurs in the vertical riser under the action of environmental loads such as wave, current and so on. At the same time, the vortex can be alternately formed on both sides of the riser due to the action of the current, and the vortex shedding produces a periodic variable force, which makes the riser produce "vortex-induced vibration"(VIV) in the lift direction

Foundation item: This work was supported by the National Natural Science Foundation of China (Grant No. 51709161), the Key Technology Research and Development Program of Shandong Province (Grant No. 2019GHY112061), the Research and Innovation Team of Ocean Oil and Gas Development Engineering Structure, College of Architecture and Civil Engineering, Shandong University of Science and Technology (Grant No. 2019TJKYTD01).
*Corresponding author. E-mail: lipeng@sdust.edu.cn

perpendicular to the IL direction. When the vortex shedding frequency is close to the natural vibration frequency of the riser structure, the discharge process of the vortex will be controlled by the vibration of the structure, leading to the phenomenon of "lock-in" resonance. The lock-in phenomenon will cause the riser to vibrate strongly and the amplitude of the riser will increase sharply (Huang et al., 2011; Trim et al., 2005; Song et al., 2017; Xu et al., 2018b). VIV is an important factor in fatigue failure of the riser during service, especially the appearance of lock-in phenomenon, which will greatly aggravate the fatigue failure of riser.

The study of VIV has received extensive attention from many scholars and numerous excellent research results have been reported. Huera-Huarte and Bearman (2009) conducted a flexible cylindrical VIV experiment with an aspect ratio of 94.0 to study the cross-flow (CF) and in-line (IL) trajectories, and the phase difference between CF and IL was analyzed at the same time. The variation rule of the average drag force with the reduced velocity and the vibration amplitude of the riser was obtained. In addition, Wu et al. (2016) further explored the coupling mechanism of the CF and IL directions of the flexible cylindrical VIV. The mass ratio and the external form of the riser are both important parameters that affect the VIV characteristics of the riser. Huera-Huarte et al. (2014) found that the CF response amplitude of the structure can exceed 3.0D by the small-volume-flexible cylindrical VIV experiment with m^*=1.1. Li et al. (2020) used discrete helical strakes vibration suppression devices with different helical numbers and discrete spacings as the research object, and found that the discrete helical strake can release the vortex behind the riser in multiple directions, destroy the spatial correlation of the vortex from multiple dimensions, and change the distribution of the original pressure field. Li et al. (2020) studied the influence of the jet-type active vibration suppression device on the dynamic response of the riser, and found that the coupling relationship between the excitation spacing and the reduced velocity is the key factor for the air curtain to enter the strong turbulence zone to achieve the best turbulent vibration suppression. In ocean engineering, the distribution of outflows is often different due to various sea areas in which the risers are located. At present, for the experimental study of riser VIV, the simulated outflow flow field can be divided into three categories: uniform flow, shear flow and stage flow. Uniform flow and shear flow are generally achieved by dragging and rotating the riser model in a uniform flow field or in still water. For example, Song et al. (2016) experimentally observed the riser VIV with L/D=1750 under uniform flow in an indoor towed pool; Xu et al. (2018a) characterized the multimodal VIV of a flexible cylinder with uniform flow and studied the effect of the rotation angle on the multi-modal response of the flexible cylinder. Lie and Kaasen (2006) conducted a VIV experiment of a flexible riser 90.0 m long under shear flow conditions and described the modal analysis method for experimental data analysis. Srinil (2011) studied the distributed diffusion wake oscillator model of VIV with variable tension vertical riser under linear shear flow. In actual engineering, the risers are not completely immersed. When entering the water from the offshore platform, there will always be a transition area between water and air. In this transition area, the surface flow field changes greatly, which will also affect the dynamic response of the riser. Based on this, some scholars have studied the dynamic response of risers with different immersion depths. Among them, Huera-Huarte et al. (2011) studied the experiment of two vertical cylinders arranged side by side. In the experiment, only the lower 40% of the cylinder was immersed in water. The experiment changed the flow velocity of the free flow, the natural frequency of the system and the spacings between the models; VIV and wake coupled VIV (WCVIV) could be identified, and the amplitude, frequency and phase synchronization between the models were given. They also used the same design concept to measure curvature with 11 strain measuring points distributed along the axis on the model with an immersion depth of 35%, and obtained a wide range of data sets. Five response models were observed, and the model with the lowest mass ratio showed the largest amplitude exceeding 3 diameters.

Based on the above description, there are few reports on the existing riser VIV experiments on the response of riser VIV under different excitation water depths. Therefore, in this paper, the VIV experiment of the riser was carried out with different excitation water depths, and the dominant frequency and dimensionless displacement of the riser under different excitation water depths are explored. The law of dynamic response parameters reveals the sensitive characteristics of the riser under different excitation water depths. The research results have important research significance and reference value for exploring the law of the VIV of deep-sea risers.

2 Experimental set-up

2.1 Description of the experimental facility

The experiment was carried out in the wave-current combined flume in the Engineering Hydrodynamics Laboratory of Ocean University of China. The section size of the water flume is 1.0 m×1.2 m, the maximum working water depth is 1 m, the maximum flow velocity is 1 m/s, and the maximum wave height is 0.3 m. In this experiment, the working water depth is 0.4−0.88 m, the outflow velocity is 0.1−0.6 m/s. The test device was placed in the flume at the distance of 22 m from the flow generator to ensure a smooth uniform flow in the test. The overall layout of the test device and flume is shown in Fig. 1.

According to the requirements of the test design, self-designed supporting device meets the test requirements. The supporting device can effectively fix the riser in the flume

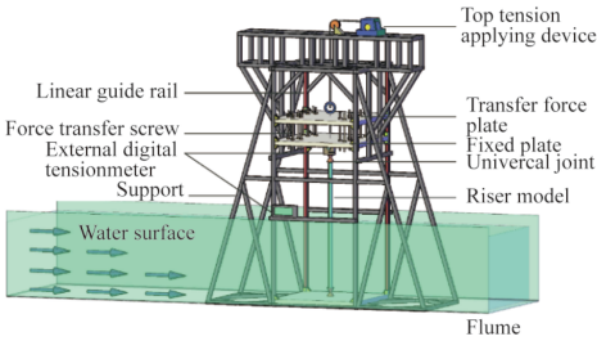

Fig. 1. Overall layout of the test device and flume.

and exert the exact initial tension. The supporting device mainly includes the transverse, longitudinal and oblique supporting structure, the applied force device, the fixed force transfer plate structure, the top tension application system, and the linear guide moving device. The supporting device was assembled from aluminum profiles, and each part of the profile was connected by high-strength T-bolts with standard and anisotropic corners. The bearing capacity check and stability test were carried out after the assembly of the supporting device to ensure the accuracy of the test data. The installation of the riser and supporting device with the actual working condition is shown in Fig. 2.

A set of top tension application system was designed, including self-locking tensioner, pulley, perforated aluminum alloy plate, AXT-S-100 tensiometer, SBR aluminum base linear guide rail and universal joint. The end of the riser was hinged boundary, the lower end of the universal joint was fixed with aluminum alloy plate by bolts, and the upper part was fixed with double gravity plates and bolts to ensure the stability and limit the torsion of the riser. From bottom to top along the riser, the top tension system was composed of universal joint, tension sensor, guiding screw, steel strand and self-locking tensioner. In order to increase the rigidity of the upper structure of the riser, two aluminum alloy plates of the same size were selected, and the fiber laser cutting technology was used for precise cutting to ensure the consistency of the opening position. The two aluminum alloy plates were rigidly connected by a force transmitting screw, the force guide screw at the upper end of the riser passes through the pores in the middle of the double aluminum alloy plates and a certain top tension was applied to the riser by adjusting the tensioner. The double aluminum alloy plate relates to the linear guide rail to ensure that the aluminum alloy plate can slide freely in the process of applying tension. The top tension value was accurately measured by a high-precision digital display tensiometer with an accuracy of 0.1 *N*. During the installation of the riser, the infrared locator is used for multi-directional positioning to reduce the deviation error from the preset position and to ensure the accuracy of the position of the fiber grating sensor.

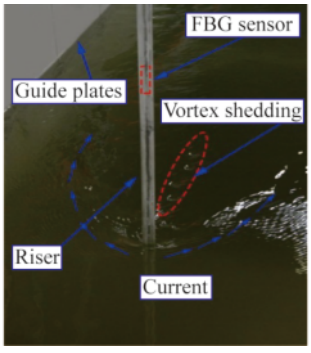

Fig. 2. Installation of riser and supporting device with actual working condition.

2.2 Riser model and test method

The test used a plexiglas tube with a length of 2 m, a wall thickness of 1 mm and an outer diameter of 18 mm as a riser model. Riser models were calibrated and produced by pipeline manufacturers, and mechanical performance tests were carried out in batches. Detailed mechanical performance parameters of riser models are shown in Table 1. In the test, the riser was standing, in which the lower part was in the uniform flow field and the upper part was in the air. The Karman vortex street phenomenon in the test is shown in Fig. 3. Specially designed joints for connecting riser, high-

Table 1 Geometric and mechanical parameters of the riser model

Parameter	Value	Unit
Total length L	2.00	m
Max Underwater length L_1	0.88	m
Max Overwater length L_2	1.60	m
Min Underwater length L_3	0.40	m
Min Overwater length L_4	1.12	m
Outer diameter D	18	mm
Wall thickness δ	1.00	mm
Mass per unit length m	0.065	kg/m
Bending rigidity EI	4.62	Nm^2
Sectional area A	53.41	mm^2
Slenderness ratio λ	111.11	–
Elasticity modulus E	2.391	GPa
Material M	PMMA	–

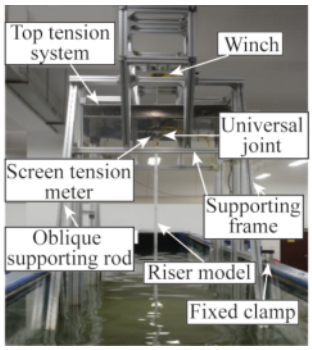

Fig. 3. Karman vortex street phenomenon of riser in flume.

quality stainless-steel materials were selected for manufacturing and assembling by professional machineries. The Fiber Bragg Grating (FBG) sensors were used in the experiment. Four bare fibers were arranged symmetrically along the surface of the riser, six grating measuring points were fabricated in each series of fibers, and four fiber grating strain sensors were arranged in 90° at each position. The vibration of the riser along the CF and IL directions were measured, respectively. Each riser model has 24 measuring points along the full length, as shown in Fig. 4a. Prior to the test, the plexiglas tube was accurately positioned by professionals to arrange the sensor and sealed along the axial length of the optical fiber sensor with α-ethyl cyanoacrylate, which effectively mitigated the interference of water flow on the optical fiber. The FBG sensor paste detail is shown in Fig. 4c.

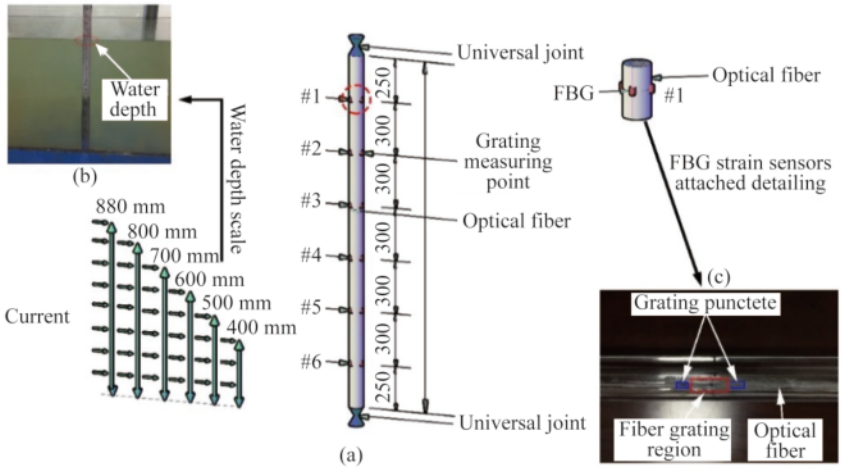

Fig. 4. Locations and arrangements of strain sensors on the surface of the riser model.

2.3 Design of VIV of the risers with different excitation water depths

In the experiment, six different water depths were designed, respectively H=0.4, 0.5, 0.6, 0.7, 0.8, 0.88 m, where H is the vertical distance from the bottom of the flume to the water surface. In order to avoid the influence of vortex discharge caused by Doppler velocimeter on the experiment and accurately measure the flow velocity, the Doppler velocimeter was placed at 2.0 m upstream of the riser, which is shown in Fig. 4a. The range of outflow velocity U is 0.1−0.6 m/s, with a total flow velocity of 10 stages. The detailed design of the test conditions is shown in Table 2.

Table 2 Working conditions of the riser model

Working conditions	Numerical number
Flow field	Stepped current of different excitation water depths
Upper part	Air
Lower part	0−0.6 m/s uniform current
Boundary condition	Articulated
Model material	Transparent poly
Riser attitude	Standing
Sampling time	40 s

3 Results and discussion

3.1 VIV frequency response analysis

When the riser is in the lock-in region, the interval of the reduced velocity U_r is usually [6.0, 7.5] (Lou, 2007). Before the formal test, the riser was placed in static water of different depths, and periodic instantaneous excitation was applied to the riser. After the excitation was released, the attenuation process of the riser vibration was observed, and the power spectrum of the riser was obtained through fast Fourier transform. According to the density curve, the 1st-order natural frequencies of the riser under different water depths in this experiment are 4.106, 3.954, 3.799, 3.549, 3.300 and 3.274 Hz, respectively. After calculation, the theoretical lock-in region outflow velocity ranges under different excitation water depths are about: [0.441, 0.552], [0.419, 0.523], [0.400, 0.501], [0.383, 0.479], [0.368, 0.460], and [0.357, 0.447].

In order to better explore the vibration characteristic frequency of the riser in and out of the lock-in region under different excitation water depths, the typical outflow velocities of 0.35 and 0.6 m/s are taken for analysis. In Fig. 5, the VIV strain time-history curve, wavelet time-frequency scale diagram and the corresponding power spectrum density distribution (a−b, c−d, e−f, g−h, i−j correspond to H=0.4−0.88 m) of the riser under different excitation water depths and at different flow velocities are drawn. The wavelet time-frequency scale diagram can directly reflect the intensity change of frequency and the change rule of characteristic frequency of VIV in the time domain. The variation

of frequency intensity under different excitation water depths is unstable versus the time. When the excitation water depth H is in the range of 0.4−0.5 m, there are many intermittent areas in the change of frequency intensity, and the intensity change of the frequency in the remaining water depth is the continuous area. When the excitation water depth H is in the range of 0.5−0.6 m, the contribution rate of the 2nd-order vibration frequency is lower than other water depths and there is no 3rd-order vibration frequency. When the excitation water depth H is in the range of 0.6−0.88 m, the intensity of the 3rd-order vibration frequency is very small. The contribution rate is very low, mainly involved in the 1st-order and 2nd-order modes. The increasing water depth will promote the excitation of high-order vibration frequency of riser structure, and the corresponding outflow velocity decreases gradually in the lock-in region. The multi-order vibration frequency is involved in the riser VIV with different excitation water depths, of which the water

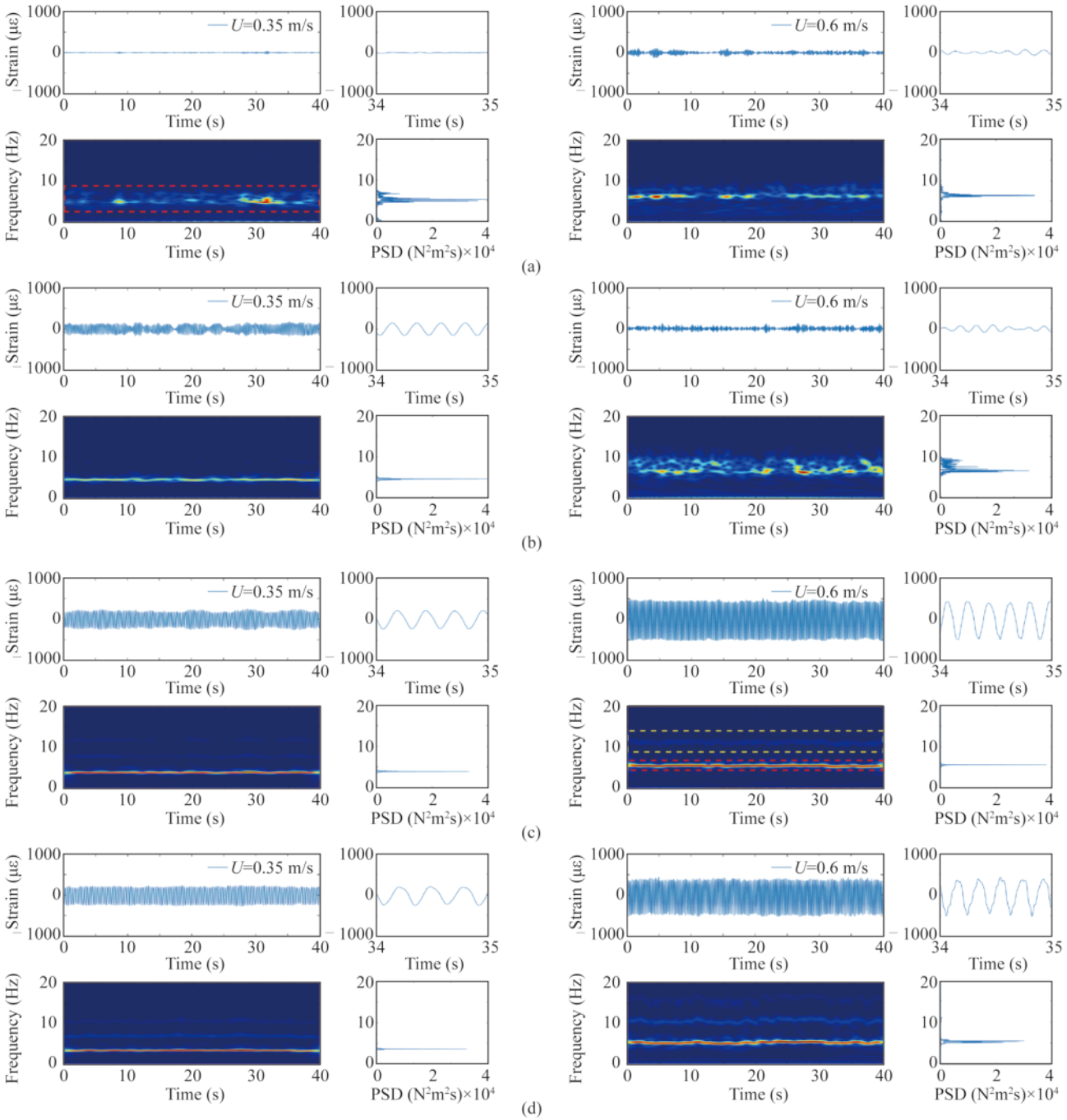

Fig. 5. Under different excitation water depths, the risers in CF direction under different flow velocities: the strain time-history curve (upper left), the strain time-history curve enlargement diagram (upper right), the wavelet time-frequency scale diagram (lower left), the power spectral density diagram (lower right), (a-f correspond to H=0.4−0.88 m). (continued on next page)

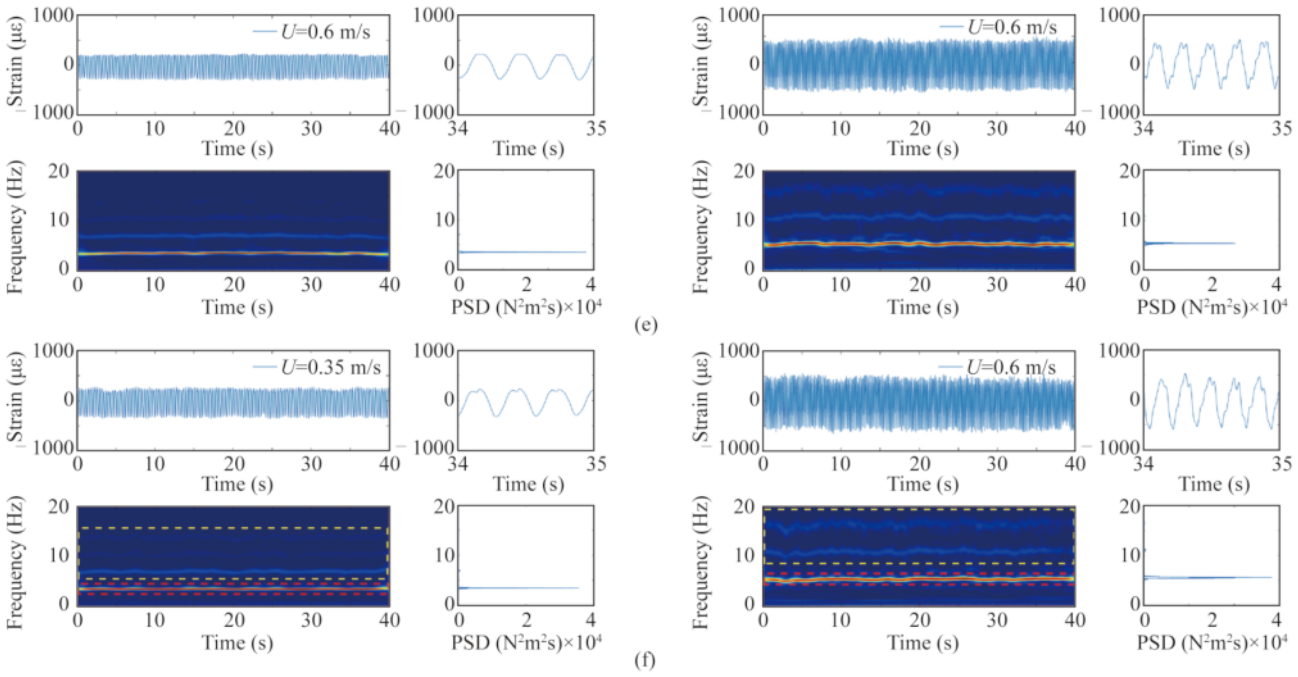

Fig. 5. (continued) Under different excitation water depths, the risers in CF direction under different flow velocities: the strain time-history curve (upper left), the strain time-history curve enlargement diagram (upper right), the wavelet time-frequency scale diagram (lower left), the power spectral density diagram (lower right), (a-f correspond to H=0.4−0.88 m).

depth H is from 0.4 m to 0.5 m, the vibration frequencies of 1st- and 2nd-order are relatively high, while those of 1st- to 4th-order are relatively high in the water depths from 0.6 m to 0.88 m. The maximum dominant mode of CF tested in this paper is 1st-order.

When the outflow velocity U is 0.35 m/s, the external excitation is small, and the intensity of vibration of the riser is weak as observed in the wavelet time-frequency scale diagram. When the excitation water depth is at 0.4 m, there is a discrete distribution of the vibration intensity in the time domain, and the vibration intensity of the riser in other excitation water depths presents a continuous distribution. When the riser is lock-in under different excitation water depths, the 1st-order vibration frequency intensity range changing with time is extremely narrow along the longitudinal direction, and remains in a red continuous region throughout the time domain, that is to say, it keeps high vibration intensity all the time. At the same time, there is a significant jump shift in the amplitude of the flow spectrum relative to the upper stage. With the increase of water depth, the flow velocity corresponding to the lock-in vibration of different excitation depths decreases gradually. It indicates that different water depths lead to differences in the additional water mass and damping, which in turn causes different external excitation strengths and leads to the difference in the corresponding velocity of the 1st-order vibration. When the outflow velocity is 0.6 m/s, the intensity of the 1st-order frequency under different excitation depths decreases significantly, while the 2nd-order vibration frequency gradually appears, but the intensity value is lower, showing a small amount of light blue discontinuous region. At this stage, the riser has jumped out of the 1st-order lock-in region and gradually approached the 2nd-order lock-in region. When the excitation water depth is 0.4−0.5 m, the 1st-order vibration frequencies are discrete and unstable, and the 1st-order vibration frequencies of other different excitation water depths remain in the continuous region. With the increase of the outflow velocity, the higher-order vibration frequency is gradually excited. The wavelet time-frequency diagram shows that the higher-order vibration frequency is lower than the lower-order vibration frequency, and the range of longitudinal distribution is wider, and the intensity of the region is lower.

In order to further explore the influence of different excitation depths on the dominant frequency and Strouhal number of the risers, Fig. 6 shows the dimensionless dominant frequency f_k/f_j (j=a, b, c, d, e, f) of the riser velocity under different excitation water depths, and the fitting lines of the dimensionless dominant frequency ratio of the riser in the IL and CF directions when the excitation water depth is 0.88 m are marked in the figure below. It should be noted that f_j is the 1st-order natural frequency at different water depths obtained by the free attenuation test, and the dominant frequency f_k in the IL and CF directions is the frequency corresponding to the peak value of the obtained power spectral density from the time-varying displacement after the fast Fourier transform, which is theoretically approximately equal to the vortex shedding frequency f_s. The least square method is used to linearly fit the CF and IL dimensionless dominant frequencies f_k/f_j with the reduced ve-

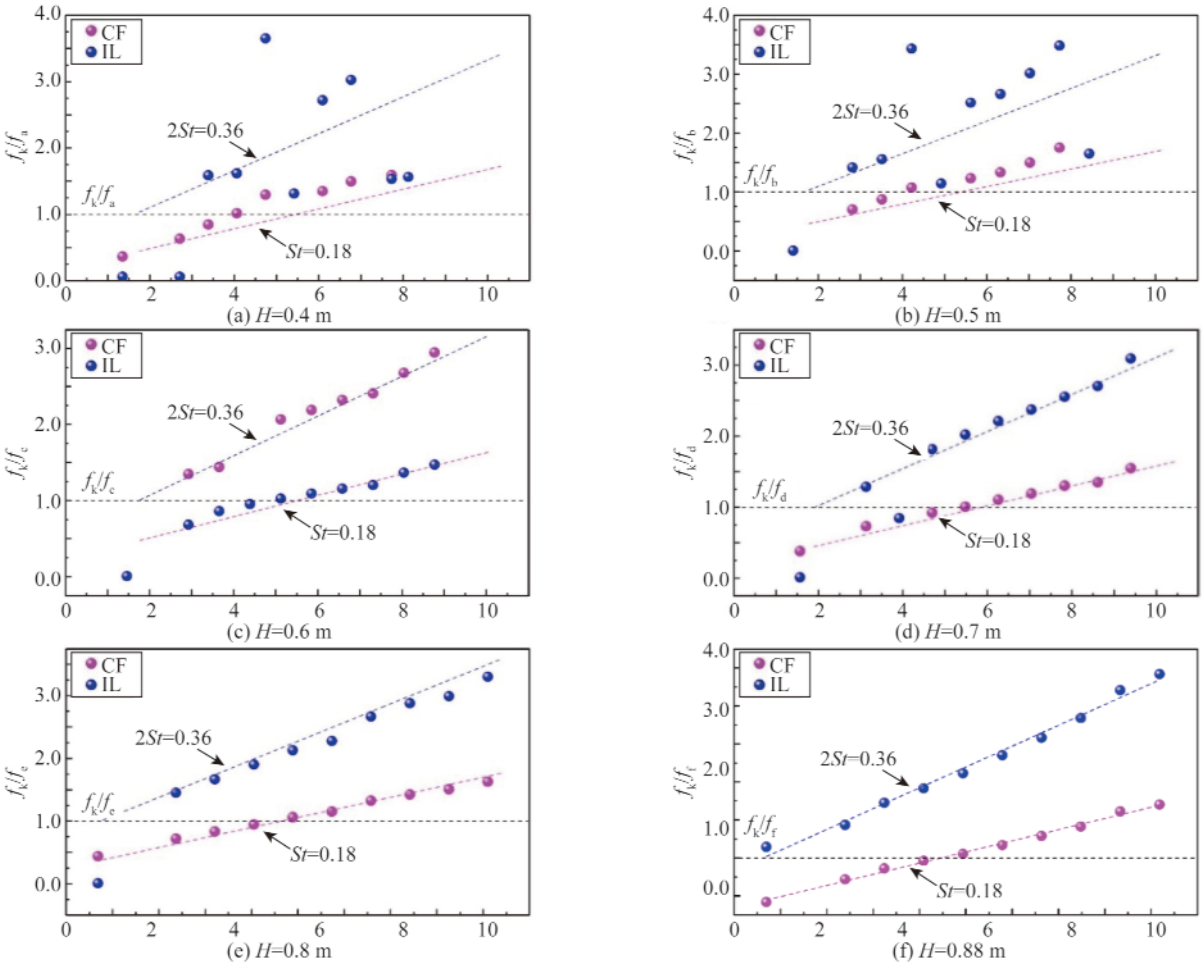

Fig. 6. Dimensionless dominant frequency in the direction of CF and IL varying with the reduced velocity and the Strouhal number fitting under different excitation water depths.

locity, where the red line represents the fitting line with the ratio of the dimensionless dominant frequency in the CF direction as the reduced velocity changes, and its slope is the representative value of Strouhal number ($St=f_sD/U=f_s/f_jU_r$), which connects the boundary layer separation and flow instability with the relatively stable vortex shedding frequency, reflecting the important parameters of the flow field in the wake area of the riser; the blue line represents the straight line fitting the dimensionless dominant frequency ratio in the IL direction with the reduced velocity.

It can be seen from Figs. 6a−6f that when the excitation water depth is 0.4−0.88 m, the dominant frequencies in the IL and CF directions have no obvious regularity in the range of reduced velocity. While the dimensionless dominant frequency of the riser in the IL and CF directions increases with the increase of reduced velocity when the excitation water depth H is between 0.8 and 0.88 m. By comparing the dominant frequency in the CF and IL directions under the six levels of water depth, it is found that the dominant frequency value of H=0.5−0.88 m is in line with the law that the IL is twice the CF direction, but when $4<U_r<9$, the excitation water depth is in the range of sudden change of 0.5−0.7 m. Interestingly, when the excitation water depth is 0.4 m, the dominant frequency ratio in the IL and CF directions is close to 1:1.5, and when the reduced velocities are 5−9, the dominant frequency decreases abruptly from the other excitation water depth, and it is entirely different from that under other excitation water depths. The results show that the external excitation intensity caused by the excitation water depth is too small, and the regularity of the riser vibration frequency is also obviously affected.

The Strouhal number of the riser under different excitation water depths has a large difference. When H=0.4 m is shown in the figure, the Strouhal number in the IL and CF direction shows a non-double relationship; while H= 0.5−0.88 m, it shows a double relationship, which conforms to the Strouhal relationship. The Strouhal number in the CF direction is close to 0.18, and the slope of the straight line fitted by the dimensionless dominant frequency is close to 0.36.

Fig. 7 shows the comparison of the instantaneous modal weight and the displacement envelope of the riser at an outflow velocity of 0.55 m/s at different excitation water depths (a−f corresponds to the excitation water depth H of 0.4 m to

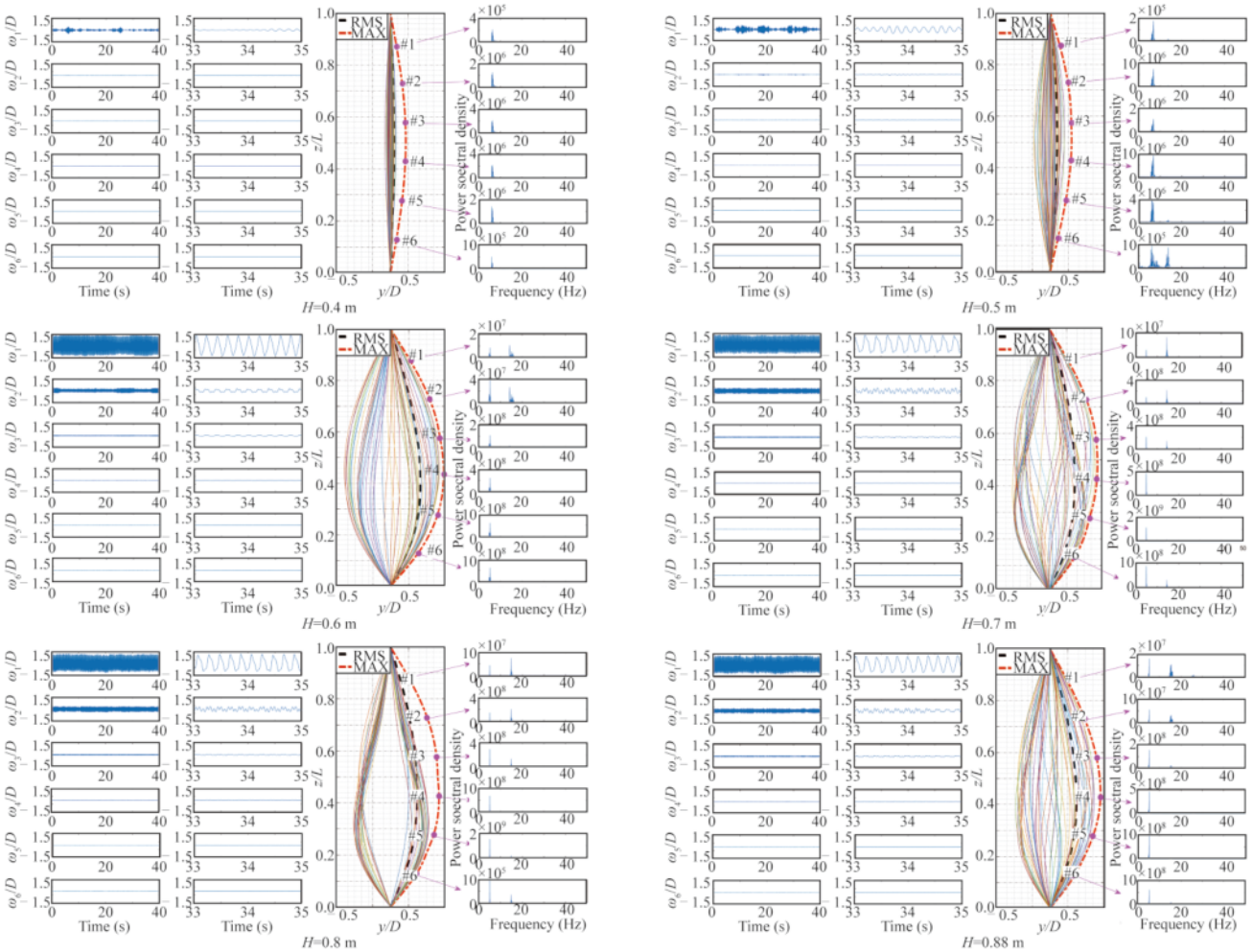

Fig. 7. First 6 orders' instantaneous modal weight curves of the riser in the direction of CF with the outflow velocity being 0.55 m/s at different excitation depths.

0.88 m). The first column shows the instantaneous curve of the six order modal weights of 0−40 s, the second column shows the six order modal weights change of 33−35 s, and the third column intercepts the displacement envelope curve of 25−35 s. At the same time, the RMS value and the maximum value of the displacement are given, which are indicated by blue and red dashed lines, respectively. The fourth column is listed as the power spectral density curve corresponding to six measuring points.

As shown by the instantaneous curves of modal weights at different excitation water depths in Fig. 7, when the excitation water depth is 0.4−0.5 m, the amplitude stability of the first order mode is larger, and the dominant mode is less stable in the whole operation process while the amplitude is about 0.36*D* and 0.5*D*. When the excitation water depth is 0.6−0.88 m, the modal contribution is maintained at a stable displacement amplitude, which is about 1.5*D*, 1.3*D*, 1.3*D*, and 1.4*D*. At the same time, with the increase of the excitation water depth, the displacement amplitude of the 2nd-order mode weight gradually increases. It can be observed from the variation of the displacement envelope diagram that when the excitation water depth is 0.4−0.5 m, only the 1st-order mode is involved, and the amplitude is low. When the excitation water depth is 0.6 m, the formation of weak 2nd-order modes is observed. And the displacement amplitude of modal weight is minimal. When the water depth is in the range of 0.7−0.88 m, the formation of the 2nd-order mode is significant with the proportion of the modal weight gradually increasing. In addition, the change of the excitation water depth has a great influence on the additional mass and external excitation of the riser. And the composite effect of the riser surface blockage and viscosity are changed while the vortex shedding of the riser in the tail vortex area affected by the mode response of the riser changed further.

3.2 VIV displacement response analysis

Fig. 8 shows the RMS dimensionless displacement versus the flow velocity in the IL and CF directions in different excitation water depths. It shows that the increase of the excitation water depth can promote the excitation of the riser VIV in the IL and CF directions. When the excitation water depth is 0.4−0.5 m, the dimensionless RMS displace-

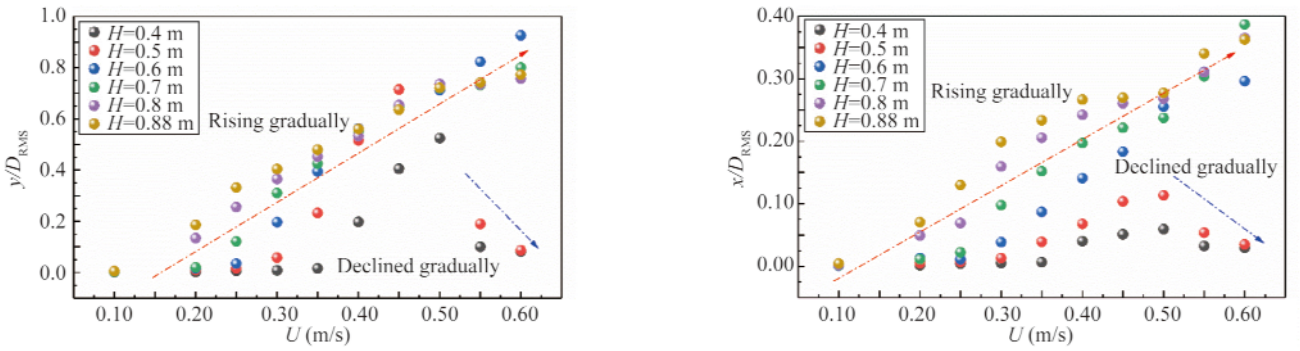

Fig. 8. RMS dimensionless displacement in the IL and CF directions versus the reduced velocity.

ment of the riser increases first then decreases with the increase of flow velocity. When the excitation water depth is in the range of 0.6−0.88 m, the dimensionless RMS displacement of the riser increases with the increase of the flow velocity. And the displacement amplitude in the CF direction is close to two times that in the IL direction in the range of the flow velocity of the whole outflow.

The red and blue dashed lines are used in the figure to describe the variation law of the dimensionless displacement of the riser under different excitation water depths. In the CF direction, when 0.1 m/s<U<0.4 m/s, the RMS displacement amplitude of risers under all excitation water depths shows a gradual upward trend, but the rate of increase varies.

When the excitation water depth is 0.6−0.88 m, the RMS amplitude of the riser displacement has not been observed to decrease substantially. As is shown in the previous analysis the riser has already reached the 1st-order lock-in vibration and gradually transitioned to the 2nd-order locking vibration in the range of the excitation depth. It is indicated that the interval of velocity selected by the experiment is large, and the drop region of the RMS dimensionless displacement value of the riser is not reflected. In the IL direction, when the excitation water depth is 0.4−0.5 m, the effect on the displacement response of the riser is also significant with relatively smooth decrease. When the excitation water depth is 0.6−0.88 m, the RMS displacement of the riser is similar to that of CF, and there is a strong linear relationship between the displacement of the riser and the velocity of outflow. Fig. 8 shows that when the outflow velocity is smaller than 0.35 m/s, the RMS dimensionless displacement amplitude of the riser is positively correlated with the excitation water depth, indicating that different excitation water depths have significant effects on the external excitation of the riser when the velocity of flow is low. When the outflow velocity is smaller than 0.35 m/s, the influence of the excitation water depth on the displacement response of the riser is no longer significant. In the IL direction, the magnitude of RMS value of dimensionless displacement of the riser coming within the experimental velocity range corresponds to the excitation water depth of 0.6 m, and its value is about 0.92D. In the CF direction, the displacement response amplitude corresponds to the excitation depth of 0.7 m. And its value is about 0.38D. The results show that with the increase of flow velocity, the external flow field of the riser is no longer a stable uniform flow field, which leads to the decrease of the influence regularity of the excitation water depth.

Fig. 9 shows the maximum value of the dimensionless displacement with the outflow flow velocity in the IL direction and CF direction under different excitation water depths. It can be seen that the influence of the RMS and the maximum value of the dimensionless displacement of the excitation water depth is similar, but the difference of the corresponding excitation water depth under the high flow velocity is relatively large. When the maximum value of di-

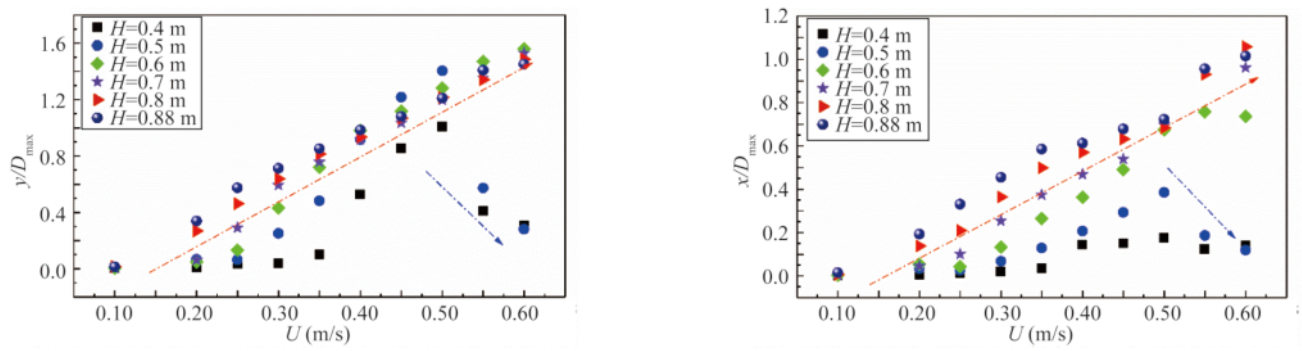

Fig. 9. MAX dimensionless displacement in the IL and CF directions versus the reduced velocity.

mensionless displacement of riser is in the CF direction while the excitation water depth is 0.4−0.5 m, it also shows a tendency of increasing first and then decreasing with the increase of outflow velocity, which is consistent with the trend of RMS dimensionless displacement which is consistent with the trend of RMS dimensionless displacement. Moreover, when the outflow velocity is larger than 0.55 m/s, the dimensionless displacement increase rate is significantly increased. When the depth of excitation water is 0.6−0.88 m, the trend of dimensionless displacement and the position of the reduced node are the same as those of the corresponding displacement, but the extent of the decrease is observed to be slightly flat. At the same time, the maximum value of dimensionless displacement of riser in the range of velocity range is consistent with the results of excitation water depth and RMS value. And its value is about 1.6*D*. In the IL direction, the trend of dimensionless displacement maximum value of riser under different excitation depths is identical to that of the RMS value conclusion, but the amplitude of dimensionless displacement maximum value corresponds to the excitation water depth of 0.8 m. And its value is about 1*D*. It can be seen from the comparison between Fig. 8 and Fig. 9 that when the outflow velocity is smaller than 0.4 m/s, the influence of the RMS value and the maximum value of the dimensionless displacement at the excitation water depth remains basically the same. However, when the outflow velocity is larger than 0.4 m/s, the influence of excitation water depth on the two is no longer regular, which indicates that the external excitation of the opposite riser under different excitation depths is difficult to keep stable at high velocity.

Figs. 10a−10d show the RMS value of the displacement of the riser at various locations along the axis of the riser at an outflow flow velocity of 0.3 m/s and 0.55 m/s. As shown the abscissa (*z*/*L*) represents the normalized riser height. Fig. 11 shows that the risers VIV with different excitation water depths is dominated by the 1st-order mode. When the outflow velocity is 0.3 m/s, the displacement along the length of the riser under different excitation water depths has positive correlation with the excitation water depth. And the amplitude in the CF and IL direction is about 0.4*D* and 0.19*D*, respectively. When the outflow flow velocity is 0.55 m/s, the effect of the excitation water depth on the displacement response along the length of the riser is no longer significant, which is consistent with the results of the analysis in Fig. 8. The higher the flow velocity is, the higher the displacement amplitude of the riser will be. The optimum vibration amplitude is obtained when the depth of excitation water is 0.6 m in the test range.

Fig. 12 shows the spatial displacement of the coupling

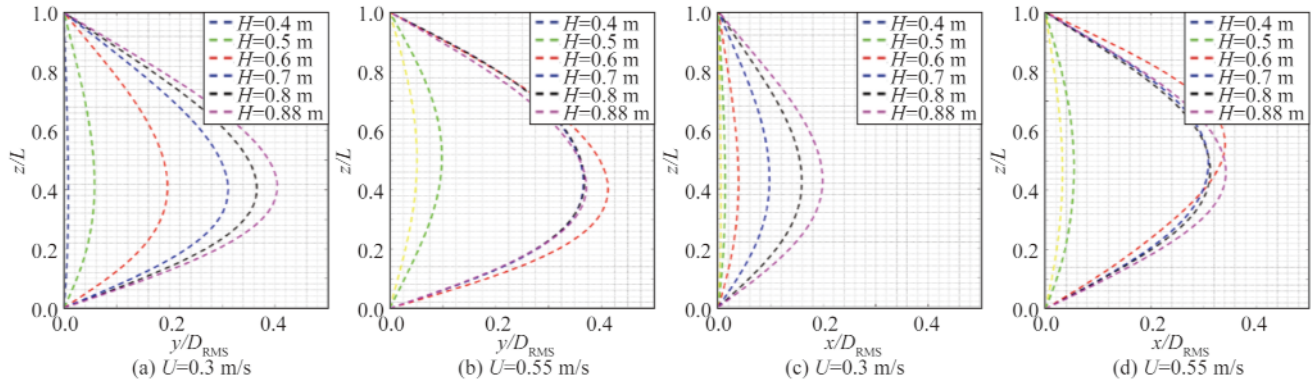

Fig. 10. RMS displacement curves along the length of riser in CF and IL directions under different excitation depths.

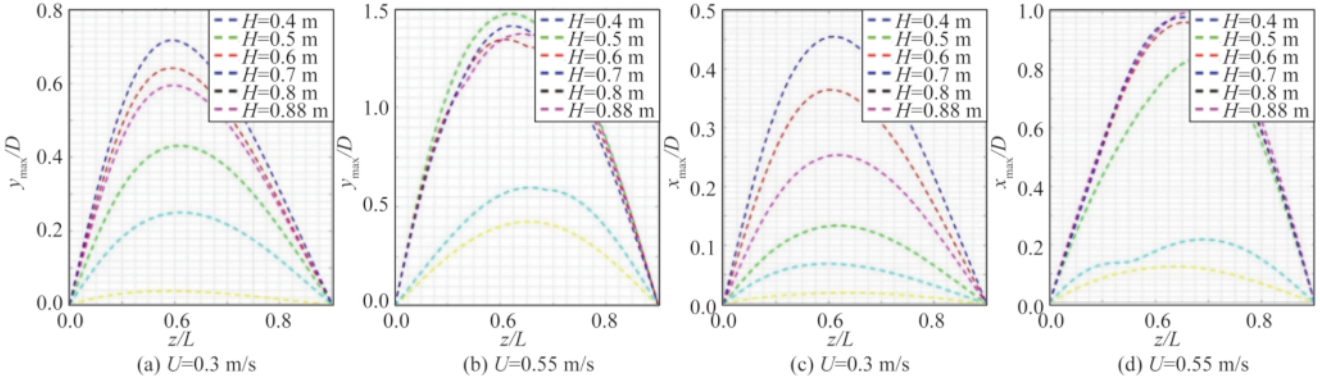

Fig. 11. Maximum curve of displacement in the CF and IL directions along the length of the riser under different excitation water depths.

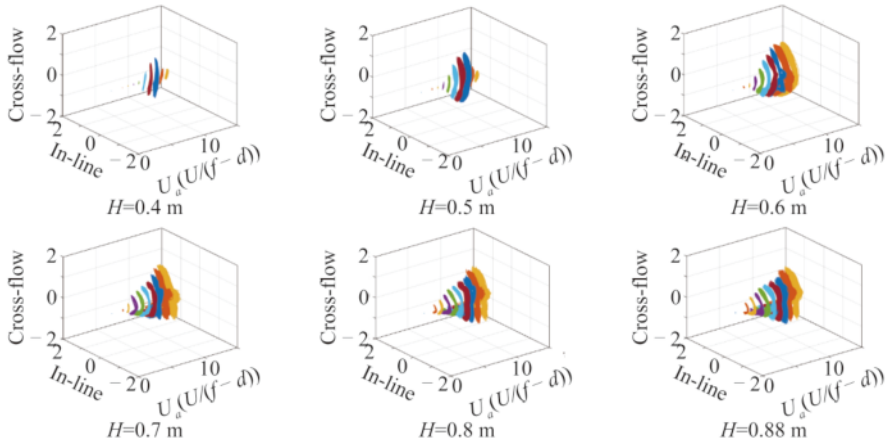

Fig. 12. Change curve of the coupling motion of the riser under different excitation water depths with the reduced velocity.

motion of the riser at the elevation of 0.4−0.88 m with the change of the reduced velocity. In order to avoid the constraint restrictions at both ends of the riser, the test proposes the measuring point #4 of the riser (Fig. 4) for analysis. In the vibration trajectory diagram of *x*-*y*-*z*, *x* stands for the reduced velocity, *y* is the IL direction, and *z* is the CF direction.

As shown in the diagram when the excitation water depth is 0.4−0.5 m, the excitation water depth is low, which reduces the nonlinear coupling action between the drag along the IL direction of the riser and the lift in the CF direction. And the trajectory of the spatial displacement is irregular with the amplitude of low displacement. When the excitation water depth is 0.6−0.7 m, the excitation water depth, and the nonlinear coupling between IL and CF increase. The spatial trajectory is gradually regular but does not show the "8" shape. When the excitation water depth is 0.8−0.88 m, the depth of excitation water increases further. And the vibration of riser under the action of lift and drag has strong nonlinear coupling while the spatial displacement trajectory presents a "8" shape. The whole analysis shows that with the reduced velocity increasing, the amplitude of the vertical riser vibration under different excitation water depths is gradually increasing. It also shows that the non-linear coupling degree of the riser vibration will be weakened with the decrease of the excitation water depth, and the "8" shape becomes more irregular.

Fig. 11 shows the maximum displacement of the riser along the axial direction of the riser when the outflow velocity of the riser is 0.3 m/s and when the outflow velocity of the riser is 0.55 m/s. When the outflow velocity is 0.3 m/s, the maximum displacement of IL and CF along the axial direction of riser at different excitation water depths is consistent with the RMS value. And the influence of the maximum depth of excitation water on the vibration displacement of the riser is significant. When the outflow velocity is 0.55 m/s, the influence of the excitation water depth on the vibration amplitude of the riser is not significant, but the displacement value of the riser corresponding to the excitation water depth is no longer consistent with the results of the analysis in Fig. 10. The corresponding excitation water depths in CF and IL direction are 0.6 m and 0.7 m, respectively.

From the comparison between Fig. 10 and Fig. 11, it is found that the spatial distribution of the RMS dimensionless displacement value and the maximum value of the riser at different excitation water depths is asymmetrical within the experimental velocity range. The main reason is that many modes take part in the VIV of the large slender riser. And the riser VIV with different excitation water depths is not the response of a single mode but the multiple vibration modes, because the participating modes are in the response mode. The difference of participating modes in frequency and phase makes the distribution of vertical riser vibration response asymmetrical in axial direction.

3.3 VIV trajectory analysis

In order to further study the dynamic response law of the coupling motion in different excitation water depths on the riser, the dynamic response law of the coupling motion is studied. Figs. 13a−13f show the coupled displacement trajectories of the riser along the direction of the outflow velocity at different excitation water depths. As can be seen from the diagram, when the depth of excitation water is 0.4−0.5 m, the displacement amplitude of the CF direction is close to that of the IL direction, which presents "O" type. When the depth of excitation water is 0.6−0.7 m, the nonlinear coupling of riser vibration is gradually enhanced, showing "C" and "X" shape respectively. At the same time, when the depth of excitation water is 0.7 m, the velocity of outflow appears to be "8" when the velocity of outflow is higher. The small number shows that the coupling vibration of the riser is unstable. When the depth of excitation water is 0.8−0.88 m, the coupling trajectory is basically in the shape of "8". Because the riser is placed in different excitation water depths, the damping state and the quality of additional

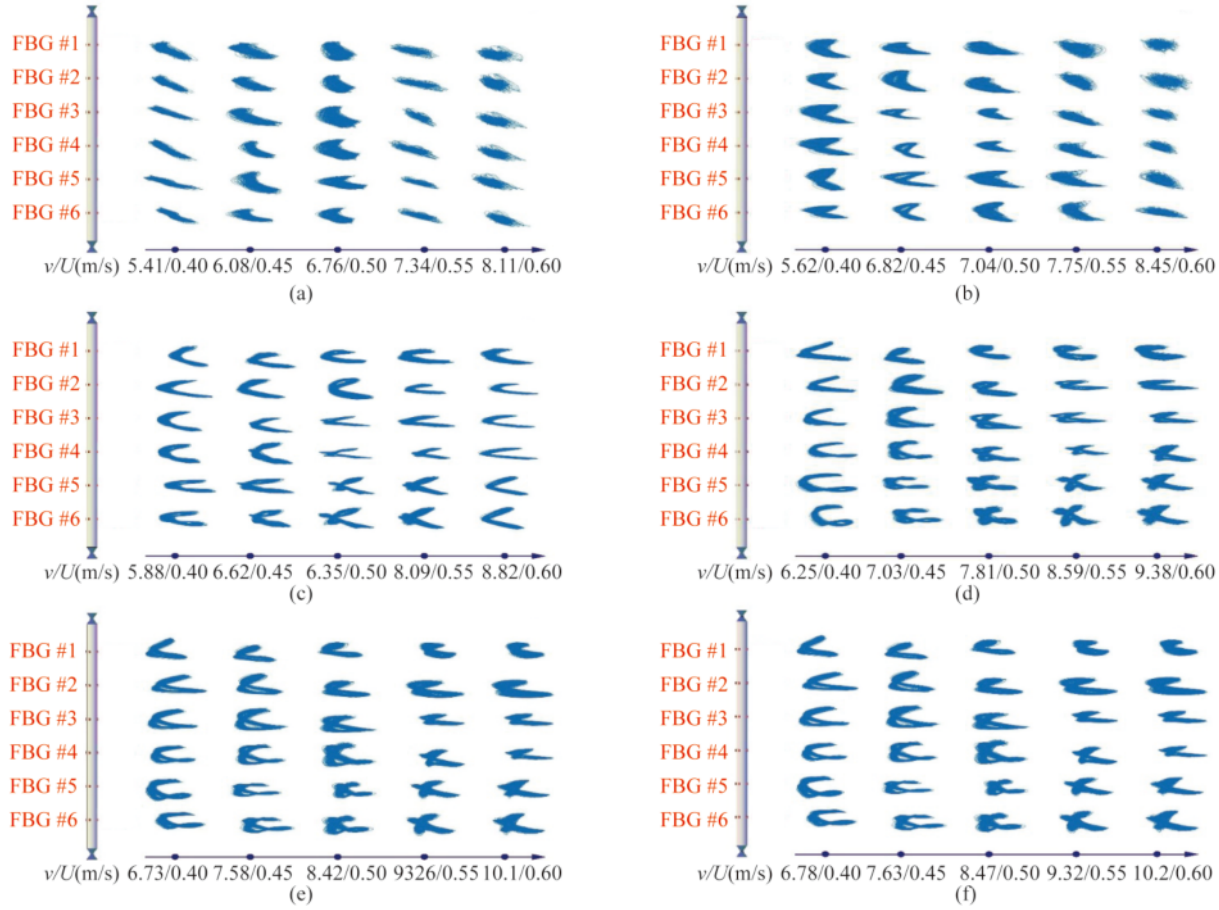

Fig. 13. Illustration of scattered points of coupling motion curve of the riser with different excitation depths.

water are different between the underwater part and the underwater part. So, the vibration amplitude and trajectory of the riser immersed under the water surface are different from those of the underwater part. According to the depth of the test design, the space of the above part is larger than that of the underwater part. Therefore, the vibration amplitude of measuring points #4−#6 under different excitation water depths is generally larger than that of measuring points #1−#3. (It should be noted that the shape of the coupled motion is given in the figure while no specific amplitude range is given).

4 Conclusions

In this paper, the VIV tests of the deep-sea riser under different excitation water depths are carried out in the water-dynamic laboratory wave-flow combined water flume, and the dynamic response of the riser VIV under different excitation water depth is studied by using the Bragg fiber grating test technique and the wavelet transform method. The following conclusions can be drawn.

(1) The change of the excitation water depth will cause the starting point of the riser lock-in region change. In the lock-in region, the vertical frequency distribution of the characteristic frequency in the time domain becomes very narrow and centered on the frequency of the lock-in frequency. The increase of the excitation water depth will reduce the corresponding outflow velocity when the vibration is locked, which will promote the high riser structure. It will promote the excitation of the high-order vibration frequency of the riser structure.

(2) The increase in the excitation water depth enhances the stability of the accelerated motion of the surrounding fluid clusters caused by the additional mass, and makes the dominant frequency and dimensionless displacement regularity of the riser more obvious at low flow velocities.

(3) The variation of the excitation water depth will cause the external excitation and additional mass changes of the riser, affecting the vortex shedding of the wake region, resulting in the same effect of the RMS value and the maximum value of the dimensionless displacement of the riser under different excitation water depths. However, the RMS and maximum amplitude of the dimensionless displacement of the riser correspond to very different excitation water depths.

(4) The difference in excitation water depth will cause the difference of external excitation at the same flow velocity, which will affect the nonlinear coupling between lift and drag, and the reduced velocity of the coupling test of the

riser in the CF and IL directions under different excitation depths. Different coupled motion trajectories are presented in the range. The riser displacement trajectory presents "O-shape", "crescent-shape", "X-shape" and "8-shape".

References

Gao, Y., Fu, S.H., Wang, J.G., Song, L.J. and Chen, Y.F., 2015. Experimental study of the effects of surface roughness on the vortex-induced vibration response of a flexible cylinder, *Ocean Engineering*, 103, 40–54.

Huang, S., Khorasanchi, M. and Herfjord, K., 2011. Drag amplification of long flexible riser models undergoing multi-mode VIV in uniform currents, *Journal of Fluids and Structures*, 27(3), 342–353.

Huera-Huarte, F.J. and Bearman, P.W., 2009. Wake structures and vortex-induced vibrations of a long flexible cylinder-Part 1: Dynamic response, *Journal of Fluids and Structures*, 25(6), 969–990.

Huera-Huarte, F.J. and Gharib, M, 2011. Flow-induced vibrations of a side-by-side arrangement of two flexible circular cylinders, *Journal of Fluids and Structures*, 27(3), 354–366.

Huera-Huarte, F.J., Bangash, Z.A. and González, L.M., 2014. Towing tank experiments on the vortex-induced vibrations of low mass ratio long flexible cylinders, *Journal of Fluids and Structures*, 48, 81–92.

Li, P., Liu, L.H., Dong, Z.K., Wang, F. and Guo, H.Y., 2020. Investigation on the spoiler vibration suppression mechanism of discrete helical strakes of deep-sea riser undergoing vortex-induced vibration, *International Journal of Mechanical Sciences*, 172, 105410.

Lie, H. and Kaasen, K.E., 2006. Modal analysis of measurements from a large-scale VIV model test of a riser in linearly sheared flow, *Journal of Fluids and Structures*, 22(4), 557–575.

Liu, C., Fu, S.X., Zhang, M.M. and Ren, H.J., 2018. Time-varying hydrodynamics of a flexible riser under multi-frequency vortex-induced vibrations, *Journal of Fluids and Structures*, 80, 217–244.

Lou, M., 2007. *Experimental Study and Numerical Simulation on the Vortex-Induced Vibration of Marine Risers Conveying Fluid*, Ph.D. Thesis, Ocean University of China, Qingdao. (in Chinese)

Song, C.H., Fu, S.X., Tang, X.Y., Hu, K., Ma, L.X. and Ren, T.X., 2018. Hydrodynamics of the semi-immersed cylinder by forced oscillation model testing, *China Ocean Engineering*, 32(1), 110–116.

Song, L.J., Fu, S.X., Cao, J., Ma, L.X. and Wu, J.Q., 2016. An investigation into the hydrodynamics of a flexible riser undergoing vortex-induced vibration, *Journal of Fluids and Structures*, 63, 325–350.

Song, L.J., Fu, S.X., Li, M., Gao, Y. and Ma, L.X., 2017. Tension and drag forces of flexible risers undergoing vortex-induced vibration, *China Ocean Engineering*, 31(1), 1–10.

Srinil, N., 2011. Analysis and prediction of vortex-induced vibrations of variable-tension vertical risers in linearly sheared currents, *Applied Ocean Research*, 33(1), 41–53.

Trim, A.D., Braaten, H., Lie, H. and Tognarelli, M.A., 2005. Experimental investigation of vortex-induced vibration of long marine risers, *Journal of Fluids and Structures*, 21(3), 335–361.

Wu, J., Lie, H., Larsen, C.M., Liapis, S. and Baarholm, R., 2016. Vortex-induced vibration of a flexible cylinder: Interaction of the in-line and cross-flow responses, *Journal of Fluids and Structures*, 63, 238–258.

Xu, W.H., Ma, Y.X., Ji, C.N. and Sun, C., 2018a. Laboratory measurements of vortex-induced vibrations of a yawed flexible cylinder at different yaw angles, *Ocean Engineering*, 154, 27–42.

Xu, W.H., Qin, W.Q. and Gao, X.F., 2018b. Experimental study on streamwise vortex-induced vibration of a flexible, *slender cylinder*, *Applied Sciences*, 8(2), 311.